A Fundamental Model for Valve Tray Vapor Cross-Flow Channeling Calculation

Jun Wang, Yixin Leng, Hui Shao, Weimin Li, Bin Xue, Chunxiang Huang, and Qian Tan
Jiangsu Key Laboratory of Advanced Catalytic Materials and Technology, School of Petrochemical Engineering, Changzhou University, Changzhou 213164, China

Ping Yang
Department of Education Research, The Institute of Education Sciences of Shenzheng, Shenzheng 518000, China

Tianxing Chen
Department of Environmental Monitoring, Safety and Environment and Technology Supervision Research Institute of Southwest Oil and Gas field Company, PetroChina, Chengdu, Sichuan 610041, China

DOI 10.1002/aic.14691
Published online November 29, 2014 in Wiley Online Library (wileyonlinelibrary.com)

An accurate prediction of tray hydraulics is very important for large diameter trays design, and vapor cross-flow channeling (VCFC) is one of the key points that affect the hydraulics calculation. Therefore, in this article, a theoretical analysis was first conducted to reveal that the energy of gas–liquid on the tray was closely related to its flow state. Then, a model was obtained on the basis of the principle of the lowest energy, which can be used to calculate VCFC. The model shows that the ratio of dry tray pressure drop to liquid height on a tray determines the gas distribution on the tray. Finally, the model was tested by comparisons with experimental results available in reference. The agreements are good. Furthermore, the effects of liquid load and fractional hole area on VCFC were studied. The results are consistent with the field experience summarized in literatures. © 2014 American Institute of Chemical Engineers *AIChE J*, 61: 1032–1042, 2015
Keywords: distillation, tray, vapor cross-flow channeling, model, energy

Introduction

Distillation is the workhorse in petroleum and/or chemistry industry.[1] In this process, the heat and mass transfer between the gas and liquid phase occurs in the valve trays. The gas distribution on the tray is one of the most important design parameters. This parameter determines the operating performance, efficiency of the gas–liquid mass transfer, and other hydraulics. On a tray, vapor is usually assumed to freely rise through the valve holes while liquid flows across the tray from the inlet downcomer to the outlet downcomer. The tray is generally considered to distribute uniformly the upflowing vapor. However, when the long liquid flow lengths, high liquid loads, and large fractional hole areas occur simultaneously, vapor may flow preferentially through the outlet of a tray. This phenomenon is called vapor cross-flow channeling (VCFC; Resetarits and Pappademos, unpublished).[2–5] Once VCFC becomes established, the vapor distribution along with the liquid flow direction will be extremely problematic. This condition can lead to excessive weeping near the tray inlet and excessive entrainment near the tray outlet.[2,3] This phenomenon can not only decrease the tray efficiencies,[6,7] but it can also lead to the tray premature entrainment flood.[2,3]

The VCFC can be avoided using multipass trays (Pilling, unpublished, Resetarits and Ogundeji, unpublished), counter-flow trays (Resetarits and Ogundeji, unpublished), and other methods (Resetarits and Pappademos, unpublished) to produce a reasonable large-diameter column with high liquid load. However, these techniques are still limited considerably by reduced tray efficiencies, increased tray costs (more complex drawings and more tray parts), longer tray installation times, and so on (Resetarits and Ogundeji, unpublished).[8] The plate structural parameters, such as flow path length, weir length, and fraction hole area, should be investigated. These parameters are important for tray designs because they significantly affect VCFC. To the best of the authors' knowledge, the rigorous method for calculation VCFC has not been reported, and only challenging results on trays (including bubble-cap, sieve, and valve trays) design have been presented for designer reference. Therefore, a model that will calculate VCFC to predict tray efficiencies and other hydraulic parameters should be established. The VCFC model will provide a theoretical guidance for reasonable design and optimization trays.

In this study, a model that can be used to predict the VCFC was constructed according to principle of lowest energy which controls the gas–liquid flow regime on the tray and on the assumption that the liquid potential energy was

Correspondence concerning this article should be addressed to J. Wang at wangjunfluid@gmail.com or Y. X. Leng at lengyixin61@163.com.

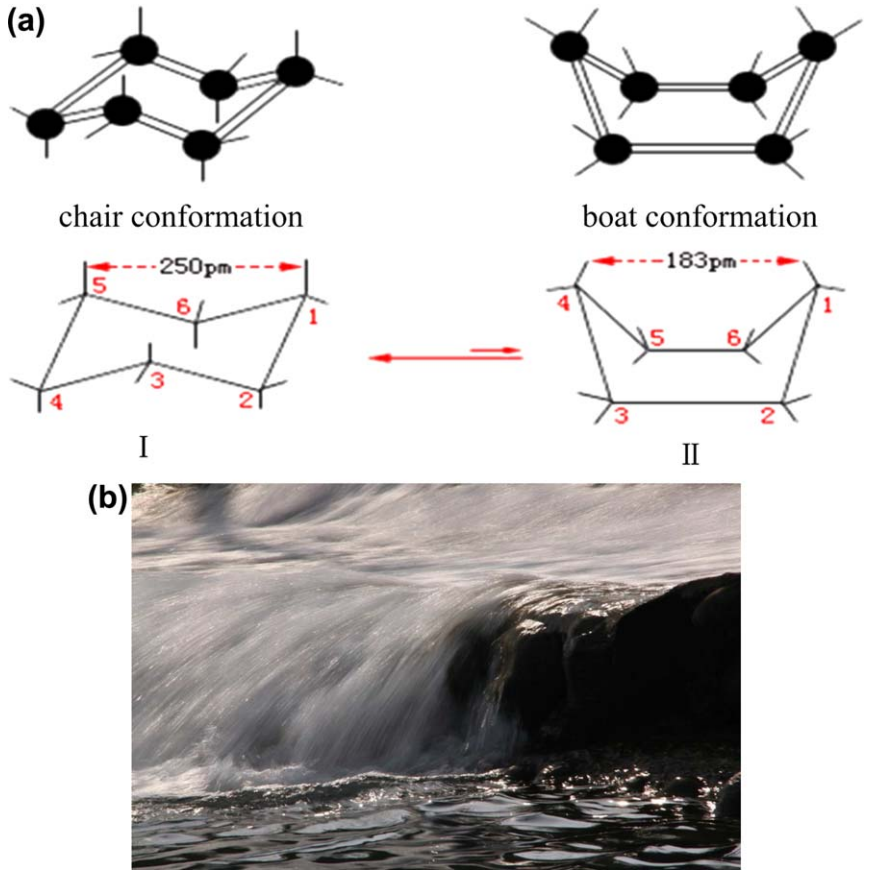

Figure 1. Relationship between nature and the principle of the lowest energy.

(a) Conformations of cyclohexane. (b) The natural flow of water. [Color figure can be viewed in the online issue, which is available at wileyonlinelibrary.com.]

much larger than the liquid kinetic energy. To solve this model, the vapor flow resistance coefficient expression and the liquid height relation between weeping and bubbling areas were established, respectively, using the theoretical analyses of the valve states and the liquid horizontal momentum balance on the tray. In addition, the model calculation program was compiled. Thus, the model can be conveniently used in practical engineering work. A verification calculation was performed to determine whether the assumption was reasonable. The calculated results were compared with previously published experimental results.

Theoretical Analysis and Modeling

Principle of the lowest energy

The principle of the lowest energy is one of the generally applicable rules in nature. This rule crucially influences the substance microstructure or direction of motion (Figure 1). Some molecules differ in conformations, and the energy of these conformations also vary. To ensure the stabilization of a system, molecules spontaneously select a conformation with minimum energy such as, at room temperature, the ratio of chair conformation of cyclohexane to boat conformation is up to approximately 10,000 (cf., Figure 1a). Meanwhile, in the macrocosm, water flows spontaneously from a high elevation to a low elevation to reduce its potential energy (cf., Figure 1b).

Generally, the gas–liquid flow regime on the tray is closely related to the operating conditions. According to energy analysis, at a certain operating condition, the gas–liquid system will spontaneously select a contact mode with lowest energy to stabilize the system. VCFC on trays is induced by an excessive hydraulic gradient in the liquid phase.[2–4,9] Indeed, this gradient promotes the vapor flowing although the tray outlet area, and ultimately, the liquid height is much higher in tray inlet area than in tray outlet area by a self-accelerating mechanism. Although, this phenomenon is not the expected flow regime, it is the most stable state at that operating condition because this contact mode is the result of the interaction of gas and liquid. The hydraulic gradient and principle of the lowest energy are not contradictory. Furthermore, the gradient may induce or accelerate the system evaluation to reach the point of lowest energy of the system.

The stability of the system depends on its energy. Therefore, the VCFC model can be established from the perspective of energy. The key points of the modeling process are the derivation of energy equations of gas–liquid flow on a tray.

Valve tray vapor cross-flow channeling model (VCFC model)

Model Establishment. The seal point[10] is a very important hydraulic point in a tray system. The full liquid fall leaks away through the valves, and no liquid flows over the outlet weir and through the downcomer as long as the operating gas velocity is equal to the seal point. Therefore, operating at this point, the weeping model selection has no effect on the calculation results of liquid weeping rate. The influence of this point operation also includes other aspects.

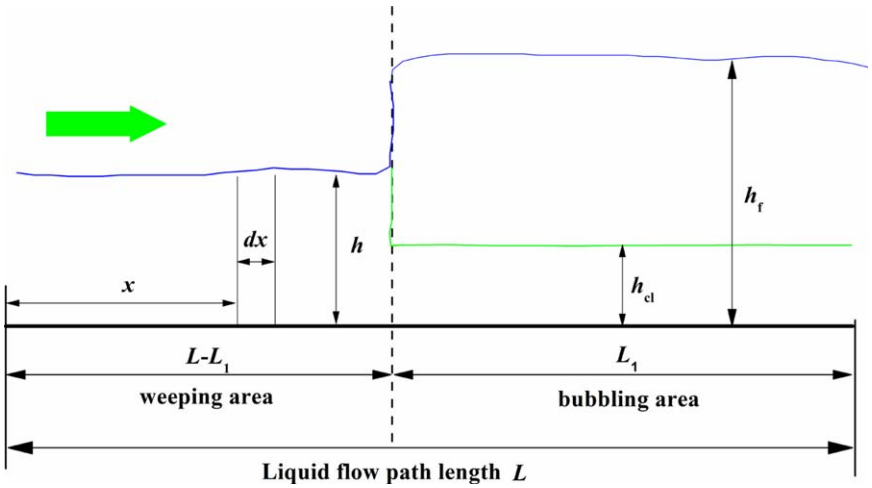

Figure 2. Schematic illustration of the two areas flow.

Green arrow indicates liquid entrance. [Color figure can be viewed in the online issue, which is available at wileyonlinelibrary.com.]

Thus, the modeling process is more convenient if the model is derived from the seal point.

The gas–liquid flow mode on the tray at the seal point is assumed to be strictly divided into two areas, namely, the weeping and bubbling areas (cf., Figure 2). The following assumptions are considered to conveniently model the system energy at this gas–liquid contact mode:

1. The vapor will flow preferentially through the outlet region of a tray when the VCFC occurs.

2. The liquid weeping rate in weeping area can be predicated by orifice equation. And the expression is

$$Q_w = \frac{nA_h(L-L_1)C_{DL}\sqrt{2(\rho_l g h - \Delta P_s)/\rho_l}}{L} \tag{1}$$

where Q_w is the liquid weeping rate, n is the valves number on a tray, A_h is the valve hole area, L is the liquid flow length, L_1 is the bubbling area length, C_{DL} is the orifice coefficient of the liquid flowing through the valve at closed state, ρ_l is the liquid density, g is the gravity acceleration, h is the liquid height of the weeping area, ΔP_S is the tray pressure drop.

3. Given that the gas density is much lower than the liquid density and the velocity of the bubble in the liquid is considerably lower than the gas orifice velocity, the kinetic and potential energies of gas are ignored.

Gas flows through the valve hole at a very high rate. However, once the high-velocity gas comes into contact with liquid, the interaction of the gas and liquid (momentum transfer) will transform the gas kinetic energy to the potential energy of liquid and the surface energy of gas–liquid bed, and so forth. Consequently, the gas (bubble) velocity becomes so slow that the kinetic energy of a bubble is much less than the surface energy of the bubble.[11] Therefore, the kinetic energy of gas can be ignored.

4. The liquid hold-up in bubbling area is regarded as constant.

The gas–liquid energy on the tray can be subdivided into potential, kinetic, and surface energies. The liquid potential energy of the weeping area E_{wh} is

$$E_{wh} = \frac{1}{2}\rho_l g W(L-L_1)h^2 \tag{2}$$

The liquid kinetic energy of the weeping area E_{wm} (cf., Figure 2) is

$$E_{wm} = \int_0^{L-L_1} \frac{\rho_l W h}{2}\left(\frac{Q_l - xA_h n C_{DL}\sqrt{2(\rho_l g h - \Delta P_S)/\rho_l}/L}{Wh}\right)^2 dx \tag{3}$$

The integration result of Eq. 3 is (see Appendix A for more detailed information)

$$E_{wm} = \frac{1}{6}\frac{\rho_l Q_l^2}{Wh}(L-L_1) \tag{4}$$

The surface energy of the bubbling area E_{ba} is[11]

$$E_{ba} = \frac{3\sigma}{r_b}(1-\alpha)Wh_f L_1 \tag{5}$$

where r_b is the mean bubble radius, α is the liquid hold-up, σ is the liquid surface tension, h_f is the froth height.

Equation 5 can be rewritten as (see Appendix B for more detailed information)

$$E_{ba} = \frac{3\sigma W L u_s h^{0.5}\alpha^{0.25}}{r_b g^{0.5}} \tag{6}$$

The gas–liquid mixture potential energy E_{bh} of the bubbling area is

$$E_{bh} = \frac{1}{2}\left[\alpha\rho_l + (1-\alpha)\rho_g\right] g W L_1 h_f^2 \tag{7}$$

As mentioned-above, the gas energy including the gas kinetic and gas potential energies can be neglected. Then, substitution of Eqs. B2 (cf., Appendix B) and (C8) (cf., Appendix C) into Eq. 7 yields

$$E_{bh} = \frac{1}{2}\rho_l g W L_1 h^2 \tag{8}$$

The gas–liquid energy on the tray is the sum of the Eqs. 2, 4, 6, and 8. The total energy can be expressed as

$$E_s = \frac{1}{2}\rho_l g W(L-L_1)h^2 + \frac{1}{6}\frac{\rho_l Q_l^2}{Wh}(L-L_1) + \frac{3\sigma W L u_s h^{0.5}\alpha^{0.25}}{r_b g^{0.5}} + \frac{1}{2}\rho_l g W L_1 h^2 \tag{9}$$

Equation 9 can be simplified as

$$E_s=\frac{1}{2}\rho_l g W L h^2+\frac{1}{6}\frac{\rho_l Q_l^2}{Wh}(L-L_1)+\frac{3\sigma W L u_s h^{0.5}\alpha^{0.25}}{r_b g^{0.5}} \quad (10)$$

Equation 10 can be further simplified as

$$e_s=\frac{1}{2}\rho_l g W h^2+\frac{1}{6}\frac{\rho_l Q_l^2}{Wh}(1-\varphi_1)+\frac{3\sigma W u_s h^{0.5}\alpha^{0.25}}{r_b g^{0.5}} \quad (11)$$

with $e_s=E_s/L$, $\varphi_1=L_1/L$. Where e_s is the total energy per meter of the tray, φ_1 is the fractional bubbling area.

To ensure the system at the stable state, its energy will achieve the lowest point by adjusting the fractional bubbling area φ_1, then Eq. 12 can be obtained

$$\frac{de_s}{d\varphi_1}=d\left(\frac{1}{2}\rho_l g W h^2+\frac{1}{6}\frac{\rho_l Q_l^2}{Wh}(1-\varphi_1)+\frac{3\sigma W u_s h^{0.5}\alpha^{0.25}}{r_b g^{0.5}}\right)/d\varphi_1=0 \quad (12)$$

Equation 12 can be rewritten as

$$\frac{dh}{d\varphi_1}=\frac{\rho_l Q_l^2/6Wh}{\rho_l g W h-\rho_l Q_l^2(1-\varphi_1)/6Wh^2+3\sigma W u_s\alpha^{0.25}/2r_b(gh)^{0.5}} \quad (13)$$

Operating at seal point ($Q_w=Q_l$), the liquid height h of the weeping area can be obtained from the orifice equation. That is

$$h=\frac{1}{2g}\left[\frac{Q_l}{A_h n C_{DL}(1-\varphi_1)}\right]^2+\frac{\Delta P_s}{\rho_l g} \quad (14)$$

The ΔP_S can be calculated by

$$\Delta P_s=\frac{1}{2}\rho_g\left(\frac{u_s}{\eta\varphi_1 C_{Dg}}\right)^2+\rho_l g h_{cl} \quad (15)$$

where η is the fractional hole area, u_s is the superficial gas velocity, C_{Dg} is the apparent orifice coefficient.

Differentiating Eq. 14 with respect to variable φ_1 gives

$$\frac{dh}{d\varphi_1}=\frac{1}{g}\left[\frac{Q_l}{A_h n C_{DL}}\right]^2\frac{1}{(1-\varphi_1)^3}-\frac{\rho_g(u_s/\eta)^2}{\rho_l g C_{Dg}^2\varphi_1^3}+\frac{dh_{cl}}{d\varphi_1} \quad (16)$$

Substitution of Eq. C8 (cf., Appendix C) into Eq. 16 yields

$$\left(1-\alpha^{0.5}\right)\frac{dh}{d\varphi_1}=\frac{1}{g}\left[\frac{Q_l}{A_h n C_{DL}}\right]^2\frac{1}{(1-\varphi_1)^3}-\frac{\rho_g(u_s/\eta)^2}{\rho_l g C_{Dg}^2\varphi_1^3} \quad (17)$$

Substitution of Eq. 14 into Eq. 17 yields

$$\left(1-\alpha^{0.5}\right)\frac{dh}{d\varphi_1}=\frac{2(\rho_l g h-\Delta P_S)}{\rho_l g(1-\varphi_1)}-\frac{2\Delta P_d}{\rho_l g\varphi_1} \quad (18)$$

with $\Delta P_d=\frac{1}{2}\rho_g\left(u_s/\varphi_1\eta C_{Dg}\right)^2$.

Equation 18 can be rewritten as

$$\frac{dh}{d\varphi_1}=\frac{2(\rho_l g h-\Delta P_S)\varphi_1-2(1-\varphi_1)\Delta P_d}{(1-\alpha^{0.5})\rho_l g(1-\varphi_1)\varphi_1} \quad (19)$$

Substitution of the expression of $\Delta P_S=(\rho_l g h_{cl}+\Delta P_d)$ into Eq. 19 yields

$$\frac{dh}{d\varphi_1}=\frac{2[\varphi_1(\rho_l g h-\rho_l g h_{cl}-\Delta P_d)-(1-\varphi_1)\Delta P_d]}{(1-\alpha^{0.5})\rho_l g(1-\varphi_1)\varphi_1} \quad (20)$$

Equation 20 can be rewritten as

$$\frac{dh}{d\varphi_1}=\frac{2[\varphi_1(\rho_l g h-\rho_l g h_{cl})-\Delta P_d]}{(1-\alpha^{0.5})\rho_l g(1-\varphi_1)\varphi_1} \quad (21)$$

Substitution of Eq. 21 into Eq. 13 yields

$$\frac{2[\varphi_1\rho_l g(h-h_{cl})-\Delta P_d]}{\rho_l g(1-\alpha^{0.5})(1-\varphi_1)\varphi_1}=\frac{\rho_l Q_l^2/6Wh}{\rho_l g W h-\rho_l Q_l^2(1-\varphi_1)/6Wh^2+3\sigma W u_s\alpha^{0.25}/2r_b(gh)^{0.5}} \quad (22)$$

The $\rho_l Q_l^2(1-\varphi_1)/6Wh^2$ and $3\sigma W u_s\alpha^{0.25}/2r_b(gh)^{0.5}$ involved in Eq. 22 represent the liquid kinetic energy of the weeping area and the surface energy of the bubbling area, respectively. The existence of the outlet weir on the tray will increase the liquid height and decrease the liquid flow velocity. At the same time, the consumed energy to form interfacial area is a small percentage of the tray pressure drop. Therefore, the liquid kinetic and surface energies are markedly lower than the liquid potential energy. Therefore, $\rho_l Q_l^2(1-\varphi_1)/6Wh^2$ and $3\sigma W u_s\alpha^{0.25}/2r_b(gh)^{0.5}$ can be ignored in Eq. 22. In addition, these two kinds of energy may balance out because the liquid kinetic energy is negative and surface energy is positive. Consequently, Eq. 22 can be simplified as

$$\frac{[\varphi_1\rho_l g(h-h_{cl})-\Delta P_d]}{(1-\alpha^{0.5})(1-\varphi_1)\varphi_1}=\frac{\rho_l Q_l^2}{12W^2h^2} \quad (23)$$

Then

$$A\varphi_1^2+(B-A)\varphi_1-C=0 \quad (24)$$

with $A=\frac{\rho_l Q_l^2(1-\alpha^{0.5})}{12W^2h^2}$, $B=\rho_l g(h-h_{cl})$, $C=\Delta P_d$.

The root of Eq. 24 with the physical meaning is

$$\varphi_1=\frac{-(B-A)+\sqrt{(B-A)^2+4AC}}{2A} \quad (25)$$

Equation 25 can be rewritten as

$$\varphi_1=\frac{-(B-A)+(B-A)\sqrt{1+4AC/(B-A)^2}}{2A} \quad (26)$$

The final form of φ_1 is (see Appendix D for more detailed information)

$$\varphi_1=\left(\frac{\frac{1}{2}\rho_g\left(u_s/\eta C_{Dg}\right)^2}{\rho_l g(h-h_{cl})}\right)^{\frac{1}{3}} \quad (27)$$

with $0\le\varphi_1\le 1$, and if $\varphi_1>1$, $\varphi_1\equiv 1$.

The left-hand side of Eq. 27 is the dimensionless variable. The conclusion, thus, obtained is that the fractional bubbling area is equal to the cube root of the ratio between the pressure drop that gas flow through the valve to the static liquid difference between the weeping and bubbling areas.

The aforementioned energy analysis suggests that φ_1 operating at seal point satisfies Eq. 27. In the case of the weeping fraction <100%, however, an energy analysis of the gas–liquid on the tray is difficult to conduct. For convenience, φ_1 at any operating condition is assumed to always conform to the aforementioned conclusion. The detailed calculation methods of the unknown parameters (C_{Dg}) or variables (h and h_{cl}) involved in Eq. 27 are discussed in other sections. In addition, if we make a change on Eq. D2 yields

$$\rho_l g\varphi_1(h-h_{cl})=\Delta P_d \quad (28)$$

The final form of Eq. 28 can be given (see Appendix E for more detailed information)

$$\varphi_1 = \frac{1}{1+\sqrt[3]{\lambda}} \tag{29}$$

with $\lambda = \frac{\rho_l}{2}\left(\frac{Q_l}{A_h n C_{DL}}\right)^2 / \frac{\rho_g}{2}\left(\frac{u_s}{\eta C_{Dg}}\right)^2$.

Equation 29 is consistent with the equation proposed by Wijn.[12]

VCFC model solution

Superficial Orifice Coefficient of Gas Flowing Through the Valves. The gas flow apparent orifice coefficient is associated with the opening states of the valve on the tray. Wang[13] found three valve states, namely, closed, inclined, and open states, on the tray operating at dry tray while the states of the valve with liquid existing were not similar to those operating at dry tray, and the states are listed as follows:

1. Valves in the weeping area are closed because no gas flows through this area.
2. Some valves in the bubbling area, which are close to weeping area, are in the floating state.[14]
3. The other valves in the bubbling area are open.

Given that the valve state in the weeping area does not affect gas flow, only the valve states in the bubbling area are considered in the calculation of the resistance coefficient as gas flow through the valves. When valves are floating in the bubbling area close to weeping area, the forces acting on the valve are in balance, and the orifice coefficient continues to change with the valve floating. To calculate the dry tray pressure drop at this state, a mean orifice coefficient C_{Df} is defined. The valves are operating at open state, so the gas flow coefficient at this state is regarded as C_{Do}. Therefore, the apparent orifice coefficient (C_{Dg}) of gas flowing through the bubbling area can be calculated by[13]

$$C_{Dg} = \phi_o(C_{Do} - C_{Df}) + C_{Df} \tag{30}$$

with $\phi_o = (u_s/\eta\varphi_1 - u_{cB})/(u_{oB} - u_{cB})$, if $\phi_o > 1$, $\phi_o \equiv 1$; if $\phi_o < 0$, $\phi_o \equiv 0$.

Parameters C_{Do}, C_{Df} in Eq. 30 can be obtained by fitting the experimental tray pressure drop data. u_{oB}, u_{cB} are the velocities of valve open balance and closed balance points, respectively, which can be obtained from the experimental dry tray pressure drop data.

Liquid Hold-Up, Clear Liquid Height of Bubble Area Calculation. The gas–liquid flow state on the tray is strictly divided into two areas, that is, the bubbling area and the weeping area. Sufficient gas–liquid contact is found in the bubbling area, so the correlations available in literature can be used to calculate the clear liquid height and liquid hold-up in the bubbling area. Herein the clear liquid height correlation[15] which was based on the analysis by Dhulisa,[16] is

$$h_{cl} = 0.063\left[\frac{Q_l\varphi_1}{W u_s}\left(\frac{\rho_l}{\rho_g}\right)^{0.5}\right]^{0.2} \tag{31}$$

Liquid hold-up correlation[15] which was based on energy analyses by Azbel[17] and Kim,[18] is

$$\alpha = \frac{1}{1+12.28\left[Fr\left(\rho_g/\rho_l\right)\right]^{0.29}} \tag{32}$$

The influence of liquid weeping on clear liquid height calculation is ignored because the weeping rate of valve trays is much lower than that of the sieve tray. The effect of weeping rate on clear liquid height can be neglected for unremarkable weeping rates. Additionally, given that Eqs. 31 and 32 are empirical correlations, the application range (including valve type, plate structure parameters, and fluid flow parameters) of these two correlations should be in accordance with Ref. 15.

Liquid Height h of Weeping Area Calculation. The calculation of liquid height of the weeping area is the most important part in VCFC model. And the height can be calculated using Eq. C6 (cf., Appendix C).

Calculating Procedure. Parameters C_{Dg} and $(h - h_{cl})$ involved in Eq. 27 are unknown. Thus, an iterative solution of φ_1 equation is required. To rigorously solve Eq. 27, the calculation program is compiled as follows:

1. First step: The initial value of $(h - h_{cl})$ is provided;
2. Second step: The initial value of C_{Dg} is provided;
3. Third step: The fractional bubbling area φ_1 and the apparent orifice coefficient C_{dg} are calculated using Eqs. 27 and 30, respectively;
4. Fourth step: Whether C_{Dg} converge is determined. If C_{Dg} reaches convergence, then the next step is performed. Otherwise, the third step is repeated, and the new initial value of C_{Dg} is the result calculated using Eq. 30;
5. Fifth step: The clear liquid height of the bubbling area h_{cl}, liquid hold-up of the bubbling area α, and liquid height of the weeping area h are calculated using Eqs. 31, 32, and C6 (cf., Appendix C), respectively;
6. Sixth step: Whether the value of $(h - h_{cl})$ converge is determined. If $(h - h_{cl})$ reaches convergence, then the next step is followed. If not, then the second step was performed, and Eqs. 31 and C6 are used to calculate the new initial value of $(h - h_{cl})$.
7. Seventh step: The calculated results φ_1, h_{cl}, and so on are yielded.

Simulation Results and Discussion

Tray pressure drop calculation results

Tray pressure drop is one of the most important hydraulic parameters, which is the key point of the calculations of the downcomer backup and tray efficiencies.[19] The tray pressure drop across a tray is the sum of the pressure drop of gas across the disperser unit, ΔP_d (sieve holes or valves), and the pressure drop through the aerated mass h_{cl}. The total pressure drop can be calculated using Eq. 15. The pressure drop calculated results based on the VCFC model are shown in Figure 3, and the results are compared with previously published experimental values.[15] Three points in the above calculating process should be established.

1. Parameters u_{cB}, u_{oB} involved in the VCFC model are obtained from published experimental results shown in Figure 4, in which u_{cB} and u_{oB} are 2.60 and 7.88 m/s, respectively.
2. Parameters C_{Do}, C_{Df} are obtained by fitting the experimental tray pressure drop values, and the correlated results are 0.445 and 0.253, respectively. In this study, only two parameters are required to be fitted in the VCFC model.
3. The detailed structural parameters of the tray and valve can be seen in Ref. 15.

The results calculated by VCFC model agree well with the experimental values (cf., Figure 3). However, the calculated results are obviously higher than the experimental

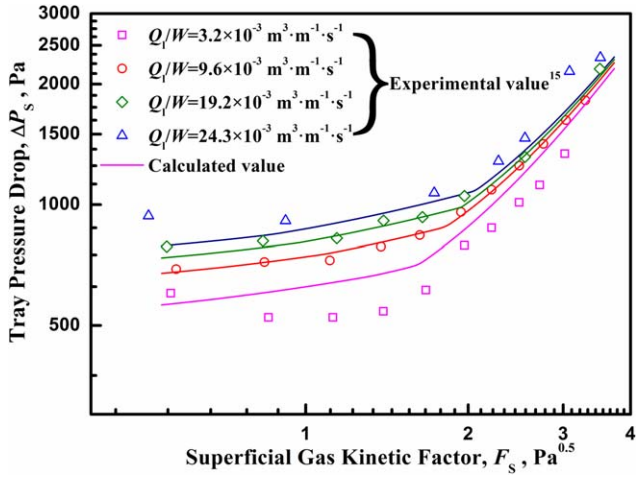

Figure 3. Comparison of the VCFC model calculation results with the experimental results.[15]

[Color figure can be viewed in the online issue, which is available at wileyonlinelibrary.com.]

values when the liquid load is $Q_l = 3.2 \times 10^{-3}$ m^3 m^{-1} s^{-1}. This condition may be due to the fact that the VCFC may not occur in this liquid load with the tray parameters given in the Ref. 15 while the tray pressure drop operating at this condition is rigorously calculated at this gas–liquid flow state. This deviation just demonstrates that the tray pressure drops operating at VCFC state are higher than those operating at the idea flow state as expected.[3] The calculated tray pressure drops at different liquid loads (cf., Figure 3) have a trend of convergence with increasing superficial gas velocity. This phenomenon occurs because the clear liquid height decreases with increasing gas velocity, and the dry tray pressure drop gradually becomes the dominant part in calculation of the total pressure drop.

In addition, Figure 3 shows that the predicted transition points of tray pressure drop are in good agreement with the experimental values. This transition point can be regarded to be a weep point (i.e., the liquid stops leakage), thus the VCFC model can be used to predict the weep point of the valve tray. Figure 3 shows that the gas velocity of the weep point increases with an increase in the liquid load. Conversely, the VCFC seems more likely occur at the high liquid load.

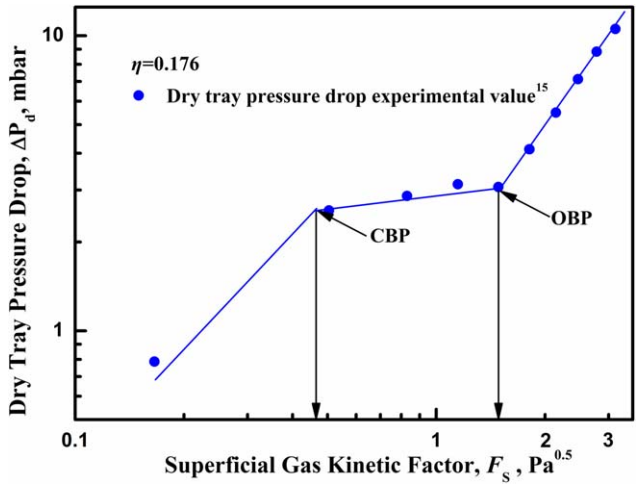

Figure 4. Experimental dry tray pressure drop values.[15]

[Color figure can be viewed in the online issue, which is available at wileyonlinelibrary.com.]

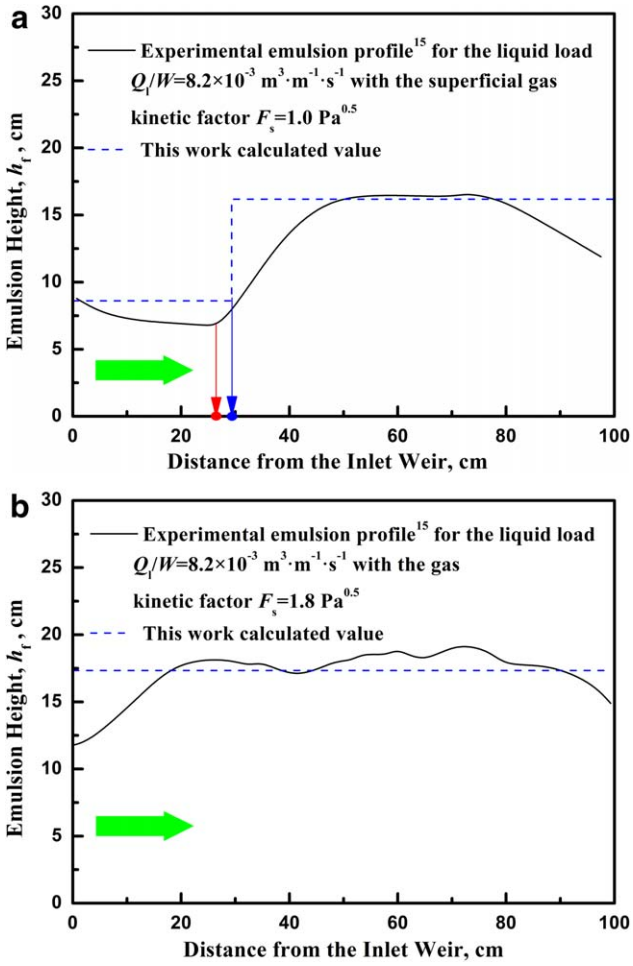

Figure 5. Comparisons of the results calculated by VCFC model with the experimental results.[15]

Green arrow indicates liquid entrance. (a) Operating at low gas rate. (b) Operating at high gas rate. [Color figure can be viewed in the online issue, which is available at wileyonlinelibrary.com.]

Emulsion height and clear liquid height profiles calculation results

The emulsion profiles at different operation velocities are predicted using the VCFC model. The results are shown in Figure 5. The predicted profiles are in a good agreement with the experimental profiles (Figure 5a). Although, the predicted froth heights in the bubbling and weeping areas are slightly larger than experimental values operating at the gas velocity of 1.0 Pa$^{0.5}$ (cf., Figure 5a), the gas–liquid flow state (i.e., VCFC) is successfully predicted. Furthermore, the junction point of the weeping and bubbling areas (i.e., fractional bubbling area) predicted by the VCFC model is in a good agreement with the experimental result (cf., Figure 5a). As the superficial gas velocity is 1.8 Pa$^{0.5}$, the model prediction result shows that the VCFC would not occur, which is in accordance with the experimental results. In addition, the predicted profile is also consistent with the experimental profile (cf., Figure 5b). These comparative results suggest that the VCFC model proposed in this study can be used to predict the valve tray VCFC.

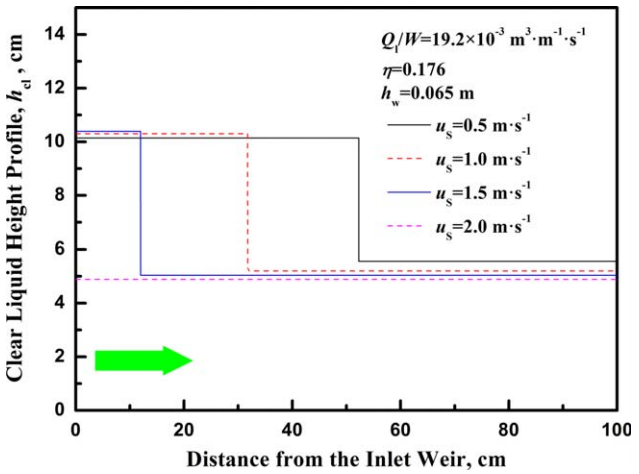

Figure 6. The effect of the superficial gas velocity on clear liquid height profile.

Arrow indicates liquid entrance. [Color figure can be viewed in the online issue, which is available at wileyonlinelibrary.com.]

The clear liquid height profiles were predicted using the VCFC model, and the results are shown in Figure 6. The VCFC is obviously observed in the case of low gas velocity. The liquid height is much higher in the weeping area than in the bubbling area when VCFC occurs. Kister[3] stated that once the gas channel is formed in a region, the gas flow resistance will be evidently reduced because of the reduction of the clear liquid height. This condition facilitates the gas flow through this area, and this operation state becomes more stable. The liquid heights of the weeping and bubbling areas slightly change with increasing superficial gas velocity, and the VCFC disappears when the superficial gas velocity is approximately 2.0 m s^{-1} (cf., Figure 6).

As stated earlier, the liquid potential energy is much larger than the liquid kinetic energy. Based on this assumption, some simplifications were performed to simplify the derivation process. The expressions of the liquid potential and kinetic energies involved in the simplification process are listed in Table 1. The ratio of the liquid potential energy to the liquid kinetic energy is obtained using the VCFC model, and the results are shown in the Figure 7. Figure 7a (the ratio of the two types of energy involved in Eq. 22) suggests that the potential energy is much larger than the kinetic energy. Although, the ratio decreases with the increase in the liquid load, the ratio is still more than 100 when the liquid load is approximately 40 × 10^{-3} m^3 m^{-1} s^{-1}. Given that the expressions of potential and kinetic energy involved in the second simplification is similar to those involved in the third simplification, Figure 7b is the representative result of the ratio of these two types of energy. The potential energy is remarkably larger than the kinetic energy. Therefore, the simplifications of Eqs. 22, 26, and D1 (cf., Appendix D) are reasonable.

Table 1. Summary of the Expressions of Potential and Kinetic Energies

The Formula	Potential Energy Expression	Kinetic Energy Expression
Eq. 22	$\rho_l g W h$	$\rho_l Q_l^2(1-\varphi_1)/6Wh^2$
Eq. 26	$\rho_l g(h-h_{cl})$	$\rho_l Q_l^2(1-\alpha^{0.5})/12W^2h^2$
Eq. D1	$\rho_l g(h-h_{cl})$	$\rho_l Q_l^2(1-\alpha^{0.5})/12W^2h^2$

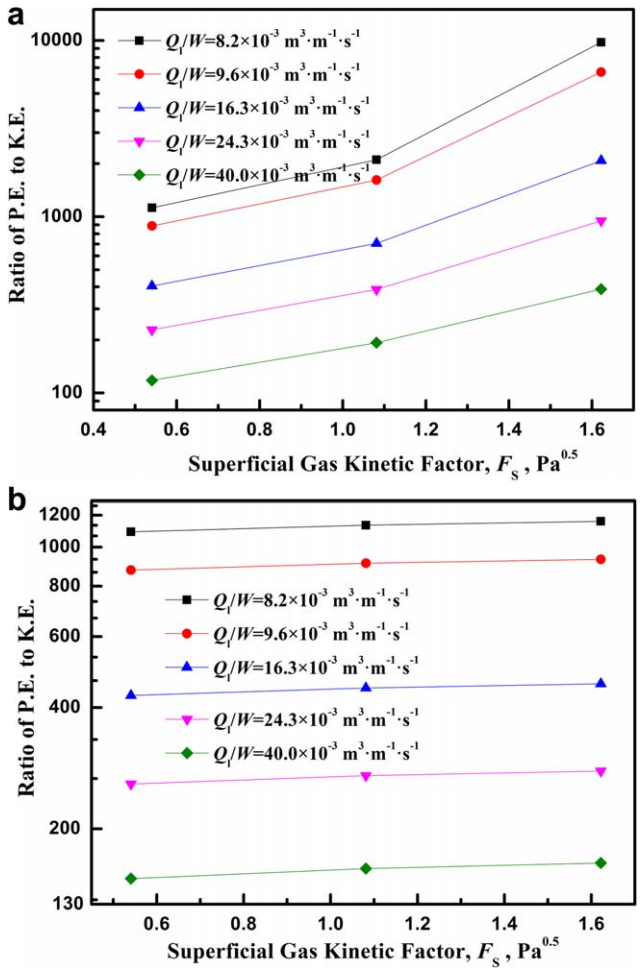

Figure 7. The ratio of the liquid potential energy to the liquid kinetic energy.

(a) The ratio of these two kinds energy involved in Eq. 22. (b) The ratio of these two kinds energy involved in Eq. 26. [Color figure can be viewed in the online issue, which is available at wileyonlinelibrary.com.]

Bubbling area fraction and open balance point calculation results

The liquid load and superficial gas velocity on fractional bubbling area are examined using the VCFC model, and the results are shown in Figure 8. The fractional hole area increases with increasing superficial gas velocity, and then, it remains constant. The velocity of the turning point is defined as the valve Open Balance Point (OBP). The higher the liquid load, the higher the superficial velocity of the valve OBP and the higher the possibility of VCFC occurrence. This result is in accordance with the field experience summarized in the literature,[3] that is, VCFC may occur when the liquid load is over 50–60 m^3 m^{-1} h^{-1}. This standpoint can also be verified by analyzing the detailed calculation results of the VCFC model.

1. Figure 8 shows that the higher the liquid load, the lower the fractional bubbling area would be. This result suggests that the gas–liquid contact condition will become undesirable with increasing liquid load. The true value of the tray efficiency is lower than the designed value expected by an

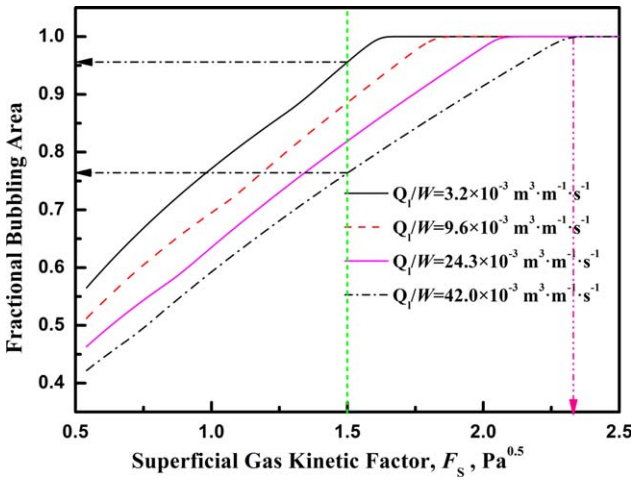

Figure 8. The effect of the liquid load on valve opening process.

[Color figure can be viewed in the online issue, which is available at wileyonlinelibrary.com.]

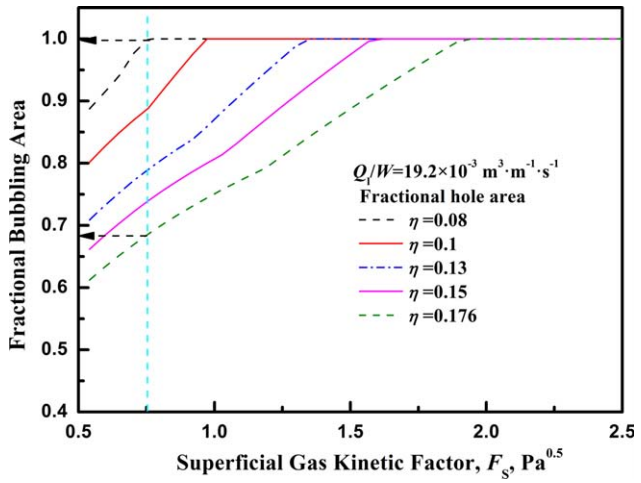

Figure 10. The effect of the fractional hole area on valve opening process.

[Color figure can be viewed in the online issue, which is available at wileyonlinelibrary.com.]

engineer, as the mal-distributed vapor flow through the tray.[20,21]

2. Generally, based on the experimental dry tray pressure drop data (cf., Figure 4), the tray operating at the condition of the superficial velocity approximately 1.5 Pa$^{0.5}$ is considered to be of good performance. However, the result calculated by VCFC model indicates that the fractional bubbling area is only approximately 0.76 at the operation condition with liquid load of approximately 42 × 10^{-3} m^3 m^{-1} s^{-1}. In this case, excessive weeping may occur in the other areas. This flow state will significantly reduce the tray efficiencies.

The VCFC model calculation results of the gas velocity of the valve OBP operating at different liquid loads are compared with the results calculated by the reference model.[15] The results are shown in Figure 9. The variation tendencies of the velocity of the valve OBP along with increasing the liquid load, which are predicted by these two models, are diametrically opposed. The VCFC model calculation results show that the OBP velocity increases with the liquid load. The results calculated by the reference model

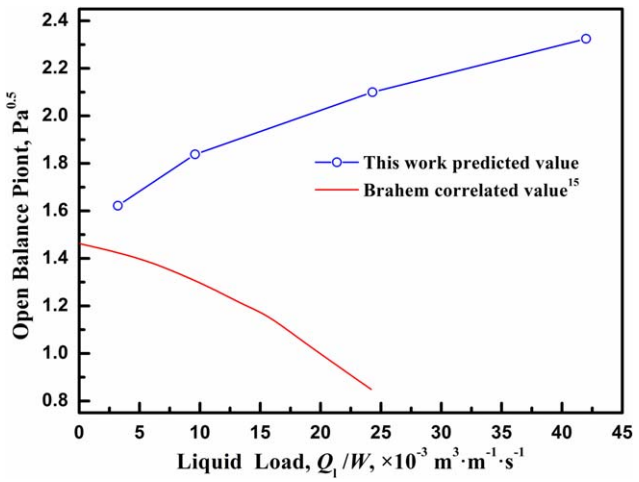

Figure 9. Comparison of the result calculated by VCFC model with the result calculated by literature model.[15]

[Color figure can be viewed in the online issue, which is available at wileyonlinelibrary.com.]

show the OBP decreasing with the increase of the liquid load. This phenomenon may have been caused by the effect of liquid horizontal velocity (horizontal inertia of the liquid on the tray) on the velocity of valve OBP that has been neglected in the current model, which is considered in the correlation of Ref. 15.

The influence of the fractional hole area on fractional bubbling area can be directly observed in Eq. 27. The φ_1 is in line with the $\eta^{-2/3}$ without considering the effect of η on the other hydraulic parameters, such as gas or liquid hold-up. The VCFC model predicted results are shown in Figure 10. Colwell's correlation[22] is used instead of Eq. 32 to calculate liquid hold-up, given that the effect of the fractional hole area on liquid hold-up has not been included in Eq. 32. Figure 10 shows that the fractional bubbling area changes dramatically with increasing fractional hole area. Furthermore, the larger the fractional hole area, the less the fractional bubbling area, such as when the fractional hole area is 0.176 with superficial velocity of approximately 0.75 Pa^5 and liquid load of approximately 19.2 × 10^{-3} m^3 m^{-1} s^{-1}, whereas the fractional bubbling area predicted by the VCFC model is only 0.68. Given that the fractional hole area is 0.08 with the same operating conditions, the predicted value shows that the gas has sufficient contact with the liquid. The comparative results indicate that the larger the fractional hole area, the more likely VCFC will occur. This conclusion is consistent with previously published field experience.[3]

Conclusion

A VCFC model that can be used to predict the VCFC of a column with large diameter and high liquid load is established. The gas and liquid on a tray can be regarded to be a system, and the stability of the system depends on its energy. The main energy on a tray includes liquid potential and kinetic energies as well as surface energy. When the energy achieves the lowest point of the system, the ratio of the dry tray pressure drop to the liquid height of a tray determines the gas distribution on the tray.

The proposed VCFC model comprises five main equations, that is, fractional bubbling area equation, dry tray pressure drop equation, liquid height of the weeping area

equation, clear liquid height of the bubbling area equation, and liquid hold-up equation. Given that the previous three equations were obtained by theoretical analyses, these models can be widely applied. The other equations are empirical correlations; therefore, the application range of these two equations should be noted. The VCFC model predicted results are compared with the experimental values (including tray pressure drop and liquid height emulsion profile), and good agreement between the two values is observed. Furthermore, the model prediction results, that is, the effects of liquid load and fractional hole area on VCFC, are consistent with published field experiences. These results reflect that the VCFC model is reasonable. Therefore, the VCFC model may provide a new way to design the column with large diameter and high liquid load.

Acknowledgment

The authors acknowledge Yang Jing for her advice and help in the theoretical aspect of model development. This work is supported by A Project Funded by the Priority Academic Program Development of Jiangsu Higher Education Institutions (PAPD).

Notation

A = intermediate variable
AA = intermediate variable
A_h = valve hole area, m^2
B = intermediate variable
BB = intermediate variable
C = intermediate variable
CC = intermediate variable
C_{DL} = orifice coefficient of the liquid flowing through the valve at closed state
C_{Df} = orifice coefficient of the gas flowing through the valve at floating state
C_{Dg} = apparent orifice coefficient
C_{Do} = orifice coefficient of the gas flowing through the valve at open state
E_{ba} = surface energy of the bubbling area, J
E_{bh} = liquid potential energy of the bubbling area, J
E_{wh} = liquid potential energy of the weeping area, J
E_{wm} = liquid kinetic energy of the weeping area, J
E_S = total energy, J
e_S = total energy per meter of the tray, J m^{-1}
Fr = Froude Number
F_s = gas kinetic factor, $Pa^{0.5}$
F_{x1} = force acting on the liquid in the bubbling area, N
F_{x2} = force acting on the liquid in the weeping area, N
g = gravity acceleration, m s^{-2}
h = liquid height of the weeping area, m
h_{cl} = clear liquid height, m
h_f = froth height, m
L = liquid flow path length, m
L_1 = bubbling area length, m
n = valves number on the tray
P_s = pressure at the liquid surface, Pa
Q_l = liquid flow rate, m^3 s^{-1}
Q_w = liquid weeping rate, m^3 s^{-1}
r_b = mean bubble radius, m
u_{cB} = velocity of the gas flowing through the valve orifice at the closed balance point, m s^{-1}
u_{oB} = velocity of the gas flowing through the valve orifice at the open balance point, m s^{-1}
u_s = superficial gas velocity, m s^{-1}
W = outlet weir length, m

Greek letters

α = liquid hold-up
ΔP_d = dry tray pressure drop with liquid existing, Pa
ΔP_S = Tray pressure drop, Pa
η = fractional hole area
λ = flow parameter
ρ_g = gas density, kg m^{-3}
ρ_l = liquid density, kg m^{-3}
φ_1 = fractional bubbling area
σ = liquid surface tension, N m^{-1}
ϕ_o = valve's number fraction of open state on the tray

Literature Cited

1. Fair JR. The workhorse today and tomorrow–distillation. *Chem Eng (NY)*. 2002;109:108–110,112.
2. Kister HZ, Larson KF, Madsen PE. Vapor cross-flow channeling on sieve trays: fact or myth? *Chem Eng Prog*. 1992;11:86–93.
3. Kister HZ. Can valve trays experience vapor cross-flow channeling? *Chem Eng*. 1993;10:18–22.
4. Hartman E. New millennium, old problems: vapor cross-flow channeling on valve trays. In: AIChE Spring National Meeting, Houston, Texas, 2001; No.2e.
5. Fair JR, Steinmeyer DE, Penney WR, Brink JA. *Chemical Engineer's Handbook*, 6th ed, Chapter 18. New York: McGraw-Hill, 1984.
6. Lockett MJ, Rahman MA, Dhulesia HA. Prediction of the effect of weeping on distillation tray efficiency. *AIChE J*. 1984;3:423–431.
7. Vybornov VG, Aleksandrov IA, Zykov DD. The effect of transverse mal-distribution of vapor and liquid flows on the operating efficiency of cross-flow trays. *Theor Found Chem Eng USSR*. 1971; 5:713–720.
8. Klemola KT, IIme JK. Effect of two-pass trays on distillation efficiencies. *Chem Eng Technol*. 1997;20:478–484.
9. Lockett MJ. *Distillation Tray Fundamentals*. London: Cambridge University Press, 1986.
10. Prince RGH, Chan BKC. The seal point of perforated distillation plates. *Trans Inst Chem Eng*. 1965;43:49–55.
11. Abzel DS. *Two Phase Flows in Chemical Engineering*. London: Cambridge University Press, 1981.
12. Wijn EF. On the lower operating range of sieve and valve trays. *Chem Eng J*. 1998;70:143–155.
13. Wang J, Tang YX, Liu YS, Cao R, Chen TX, Hu YF, Fan XJ. A new dry tray pressure drop model of float valve trays. *AIChE J*. 2013;59:2694–2705.
14. Zhang LS, Wang XZ, Xu XM, Yang JD, Shen F. A general model for correlation of weeping rates of valve-type trays. *Pet Chem Tech (China)*. 1988;7:415–419.
15. Brahem R, Lebeaud AR, Legendre D, Moreaud M, Duval L. Experimental hydrodynamic study of valve trays. *Chem Eng Sci*. 2013;100: 23–32.
16. Dhulesia H. Clear liquid height on sieve and valve trays. *Chem Eng Res Des*. 1984;62:321–326.
17. Azbel DS. The hydrodynamics of bubbler processes. *Int Chem Eng*. 1963;3:319–323.
18. Kim SK. Theoretical study of vapor-liquid hold up on a perforated plate. *Int Chem Eng*. 1966;6:634.
19. Bennett DL, Agrawal R, Cook PJ. New pressure drop correlation for sieve tray distillation columns. *AIChE J*. 1983;3:434–442.
20. Mohan T, Rao KK, Rao DP. Effect of vapor mal-distribution and entrainment on tray efficiency. *Ind Eng Chem Process Des Dev*. 1983;22:380–385.
21. Mohan T, Rao KK, Rao DP. Effect of vapor mal-distribution on tray efficiency. *Ind Eng Chem Process Des Dev*. 1983;22:376–380.
22. Colwell CJ. Clear liquid height and froth density on sieve trays. *Ind Eng Chem Process Des Dev*. 1981;20:298–307.

Appendix A: The Detailed Integration Process of Eq. 3

$$E_{wm}=\int_0^{L-L_1}\frac{\rho_l Wh}{2}\left(\frac{Q_l-xA_hnC_{DL}\sqrt{2(\rho_l gh-\Delta P_S)/\rho_l}/L}{Wh}\right)^2 dx \tag{A1}$$

Equation A1 can be rewritten as

$$E_{wm}=\int_0^{L-L_1}\frac{\rho_l}{2Wh}\left({Q_l}^2-2Q_l xA_hnC_{DL}\sqrt{2(\rho_l gh-\Delta P_S)/\rho_l}/L\right)$$

$$+\frac{\rho_l}{2Wh}x^2\left(A_h nC_{DL}\sqrt{2(\rho_l gh-\Delta P_S)/\rho_l}/L\right)^2 dx \quad (A2)$$

Equation A2 can be simplified as

$$E_{wm}=AA+BB+CC \quad (A3)$$

with

$$AA=\int_0^{L-L_1}\frac{\rho_l Q_l^2}{2Wh}dx\, BB=\int_0^{L-L_1}-\frac{\rho_l}{2Wh}(2Q_l x A_h nC_{DL}\sqrt{2(\rho_l gh-\Delta P_S)/\rho_l}/L)$$

$$dx, CC=\int_0^{L-L_1}\frac{\rho_l}{2Wh}\left(A_h nC_{DL}\sqrt{2(\rho_l gh-\Delta P_S)/\rho_l}/L\right)^2 x^2 dx$$

The respective integration results of AA, BB, CC are

$$AA=\frac{\rho_l Q_l^2}{2Wh}(L-L_1) \quad (A4)$$

$$BB=-\frac{\rho_l Q_l}{2Wh}\left(A_h nC_{DL}\sqrt{2(\rho_l gh-\Delta P_S)/\rho_l}/L\right)(L-L_1)^2 \quad (A5)$$

$$CC=\frac{\rho_l}{6Wh}\left(A_h nC_{DL}\sqrt{2(\rho_l gh-\Delta P_S)/\rho_l}/L\right)^2(L-L_1)^3 \quad (A6)$$

The liquid weeping rate is equal to the liquid flow rate operating at seal point

$$Q_l=Q_w \quad (A7)$$

The weeping rate can be calculated by orifice equation; therefore, Eq. A8 is obtained, that is

$$Q_w=A_h nC_{DL}\sqrt{2(\rho_l gh-\Delta P_S)/\rho_l}(L-L_1)/L \quad (A8)$$

Substitution of Eqs. A7 and A8 into Eqs. A5 and A6, respectively, yields

$$BB=-\frac{\rho_l Q_l^2}{2Wh}(L-L_1) \quad (A9)$$

$$CC=\frac{\rho_l Q_l^2}{6Wh}(L-L_1) \quad (A10)$$

Substitution of Eqs. A4, A9, and A10 into Eq. A3 yields

$$E_{wm}=\frac{\rho_l Q_l^2}{6Wh}(L-L_1) \quad (A11)$$

Appendix B

$$E_{ba}=\frac{3\sigma}{r_b}(1-\alpha)Wh_f L_1 \quad (B1)$$

The froth height h_f involved in Eq. B1 can be calculated by,

$$h_f=\frac{h_{cl}}{\alpha} \quad (B2)$$

where h_{cl} is the clear liquid height of the bubbling area. α can be calculated by Azbel,[17]

$$\alpha=\frac{1}{1+Fr^{0.5}} \quad (B3)$$

with $Fr=(u_s L/L_1)^2/gh_{cl}$, where Fr is Froude number.

The liquid height relation between the weeping area and the bubbling area operating at seal point is (see Appendix C for more detailed information)

$$h_{cl}=h\alpha^{0.5} \quad (B4)$$

Substitution of Eqs. B2, B3, and B4 into Eq. B1 yields

$$E_{ba}=\frac{3\sigma WLu_s h^{0.5}\alpha^{0.25}}{r_b g^{0.5}} \quad (B5)$$

Appendix C: Relationship Between h and h_{cl}

Assuming the gas distribute uniformly in liquid, we can obtain Eq. C1 in the bubbling area (seen in Figure C1), that is

$$\frac{dP}{dh_x}=-\alpha\rho_l g \quad (C1)$$

Integrating Eq. C1 (from h_x to h_f) yields

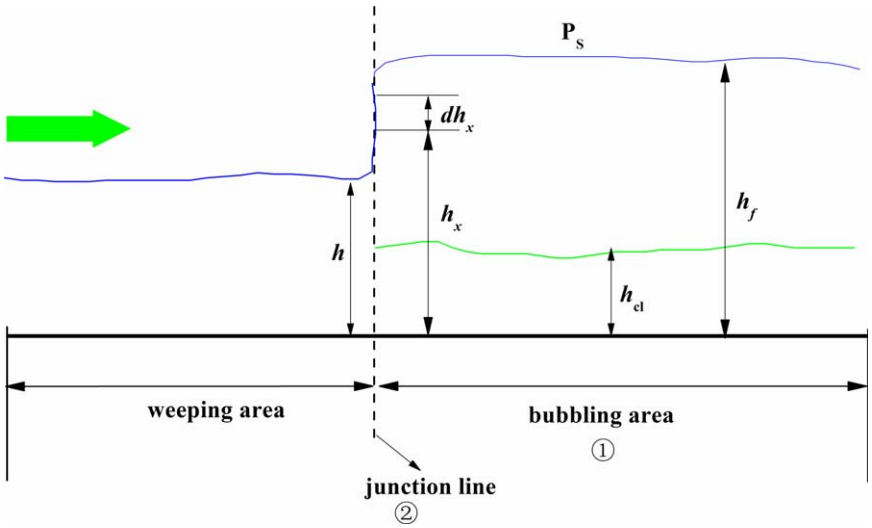

Figure C1. Schematic illustration of control sections.

Green arrow indicates liquid entrance. [Color figure can be viewed in the online issue, which is available at wileyonlinelibrary.com.]

$$P-P_s=\alpha\rho_l g(h_f-h_x) \tag{C2}$$

The force of the liquid gravity acting on the bubbling area is

$$F_{x1}=\int_0^{h_f}(P-P_s)Wdh \tag{C3}$$

Substitution of Eq. C2 into Eq. C3 and integration yields

$$F_{x1}=\frac{1}{2}\alpha\rho_l g h_f^2 W \tag{C4}$$

The force of the liquid gravity acting on the junction of the weeping area and bubbling area can be also given

$$F_{x2}=\frac{1}{2}\rho_l g W h^2 \tag{C5}$$

The liquid horizontal momentum balance equation between the junction line (cf., Figure C1) and bubbling area is

$$\frac{\rho_l Q_l^2}{h_{cl}W}+\frac{\alpha\rho_l g W h_f^2}{2}=\frac{\rho_l Q_l^2}{hW}+\frac{\rho_l g W h^2}{2} \tag{C6}$$

As the liquid flow rate is equal to the weeping rate of the weeping area operating at seal point, the liquid rate flowing through the junction line is zero. Therefore, Eq. C7 can be obtained from Eq. C6

$$\frac{\alpha\rho_l g W h_f^2}{2}=\frac{\rho_l g W h^2}{2} \tag{C7}$$

Equation C7 can be rewritten as

$$h_{cl}=h\alpha^{0.5} \tag{C8}$$

Appendix D

As previously assumed, the value of B is much larger than A. However, as the relationship between the C and $(B-A)$ is unknown, a segmentation discussion is performed to establish the final form of φ_1. The detailed information is described as follows.

In the Case of C < (B − A)

As $A<<(B-A)$, the expression $AC<<(B-A)C$ is correct. And $C<(B-A)$, then the expression $AC<<(B-A)^2$ can be established. Therefore, the expression $\sqrt{1+4AC/(B-A)^2}$ can be simplified and approximated by $1+4AC/2(B-A)^2$.

Then, Eq. 26 can be simplified as

$$\varphi_1=\frac{C}{(B-A)}\approx\frac{C}{B} \tag{D1}$$

Substitution of the expressions of B and C into Eq. D1 yields

$$\varphi_1=\frac{\Delta P_d}{\rho_l g(h-h_{cl})} \tag{D2}$$

Substitution of the expression $\Delta P_d=0.5\ \rho_g(u_s/\varphi_1\eta C_{Dg})^2$ in to Eq. D2 yields

$$\varphi_1=\frac{\frac{1}{2}\rho_g\left(u_s/\varphi_1\eta C_{Dg}\right)^2}{\rho_l g(h-h_{cl})} \tag{D3}$$

Then, Eq. D3 can be rewritten as

$$\varphi_1=\left(\frac{\frac{1}{2}\rho_g\left(u_s/\eta C_{Dg}\right)^2}{\rho_l g(h-h_{cl})}\right)^{\frac{1}{3}} \tag{D4}$$

In the Case of C = (B − A)

The expression $\sqrt{1+4AC/(B-A)^2}$ is equal to $\sqrt{1+4A/(B-A)}$. Then, Eq. 26 can be simplified as

$$\varphi_1=\frac{-(B-A)+(B-A)(1+4A/2(B-A))}{2A}=1 \tag{D5}$$

In the Case of C > (B − A)

$$\varphi_1=\frac{-(B-A)+(B-A)\sqrt{1+4AC/(B-A)^2}}{2A}>\frac{-(B-A)+(B-A)\sqrt{1+4A/(B-A)}}{2A}=1 \tag{D6}$$

The value of φ_1 should be in the range of $0\le\varphi_1\le1$. Therefore, if $\varphi_1>1$, $\varphi_1\equiv1$. As a result, in this case the value of C has no effect on calculated result of φ_1.

Based on the above analyses, the final simplified expression of φ_1 is

$$\varphi_1=\left(\frac{\frac{1}{2}\rho_g\left(u_s/\eta C_{Dg}\right)^2}{\rho_l g(h-h_{cl})}\right)^{\frac{1}{3}} \tag{D7}$$

with $0\le\varphi_1\le1$, and if $\varphi_1>1$, $\varphi_1\equiv1$.

Appendix E

Equation 28 can be rewritten as

$$\rho_l g\varphi_1(h-h_{cl})-\varphi_1\Delta P_d=(1-\varphi_1)\Delta P_d \tag{E1}$$

Then

$$\varphi_1(\rho_l gh-\Delta P_S)=(1-\varphi_1)\Delta P_d \tag{E2}$$

Substitution of Eq. 14 into Eq. E2 yields

$$\frac{\rho_l}{2(1-\varphi_1)^3}\left[\frac{Q_l}{A_h n C_{DL}}\right]^2=\frac{\Delta P_d}{\varphi_1} \tag{E3}$$

Equation E3 can be rewritten as

$$\frac{\rho_l}{2(1-\varphi_1)^3}\left(\frac{Q_l}{A_h n C_{DL}}\right)^2=\frac{\rho_g}{2{\varphi_1}^3}\left(\frac{u_s}{\eta C_{Dg}}\right)^2 \tag{E4}$$

Then

$$\varphi_1=\frac{1}{1+\sqrt[3]{\lambda}} \tag{E5}$$

with $\lambda=\frac{\rho_l}{2}\left(\frac{Q_l}{A_h n C_{DL}}\right)^2/\frac{\rho_g}{2}\left(\frac{u_s}{\eta C_{Dg}}\right)^2$.

Manuscript received Aug. 4, 2014, and revision received Oct. 2, 2014.